TELLUS

A diagnostic carbon flux model to monitor the effects of disturbance and interannual variation in climate on regional NEP

By D. P. TURNER[1]*, W. D. RITTS[1], J. M. STYLES[1], Z. YANG[1] W. B. COHEN[2], B. E. LAW[1] and P. E. THORNTON[3],   [1]*Department of Forest Science Oregon State University Corvallis OR 97331, USA;* [2]*USDA Forest Service PNW Research Station Corvallis OR 97331, USA;* [3]*National Center for Atmospheric Research Climate and Global Dynamics Division Boulder CO 80301, USA*

ABSTRACT

Net ecosystem production (NEP) was estimated over a 10.9×10^4 km^2 forested region in western Oregon USA for 2 yr (2002–2003) using a combination of remote sensing, distributed meteorological data, and a carbon cycle model (CFLUX). High spatial resolution satellite data (Landsat, 30 m) provided information on land cover and the disturbance regime. Coarser resolution satellite imagery (MODIS, 1 km) provided estimates of vegetation absorption of photosynthetically active radiation. A spatially distributed (1 km) daily time step meteorology was generated for model input by interpolation of meteorological station data. The model employed a light use efficiency approach for photosynthesis. It was run over a 1 km grid. This approach captured spatial patterns in NEP associated with climatic gradients, ecoregional differences in NEP generated by different management histories, temporal variation in NEP associated with interannual variation in climate and changes in NEP associated with recovery from disturbances such as the large forest fire in southern Oregon in 2002. Regional NEP averaged 174 gC m^{-2} yr^{-1} in 2002 and 142 gC m^{-2} yr^{-1} in 2003. A diagnostic modelling approach of this type can provide independent estimates of regional NEP for comparison with results of inversion or boundary layer budget approaches.

1. Introduction

Regional estimates of terrestrial net ecosystem production (NEP) using the inverse modelling approach (Bousquet et al., 2000) or boundary layer budget (Levy et al., 1999) approach provide 'top-down' flux estimates based on observations of CO_2 concentration. These estimates generally do not allow for close examination of possible mechanisms driving the spatial and temporal variation in NEP. 'Bottom-up' flux estimates—that take into account factors including climate, vegetation type, disturbance history and phenology—can potentially provide independent estimates of NEP that are informative with respect to mechanisms (Turner et al., 2004a). Comparisons of flux estimates from top-down and bottom-up approaches, and ultimately their combination in data assimilation modelling (Raupach et al., 2005), will be an integral part of regional assessments such as the North American Carbon Plan (Denning et al., 2005).

Bottom-up scaling approaches based on carbon cycle modelling vary widely with respect to the degree of their reliance on observations for model drivers. In purely prognostic models, initial conditions are specified only in terms of characteristics such as soil texture and depth. The model drivers are then climate data, and the model outputs include plant functional type, vegetation phenology, carbon pools and carbon fluxes—notably net primary production (NPP), heterotrophic respiration (R_h), and NEP (e.g. Stich et al., 2003). This model type can be used for scaling NEP under contemporary conditions (Schimel et al., 2000) and future climate scenarios. It yields information about possible disequilibria in carbon pools associated with climate variability and is commonly used for simulating terrestrial carbon cycle responses (feedbacks) to potential climate change (Cox et al., 2000).

At the other extreme, a diagnostic modelling approach may use similar climate data (possibly at higher spatial resolution) but also ingest information from satellite remote sensing on vegetation condition—particularly canopy absorption of solar radiation (e.g LaFont et al., 2002; Potter et al., 2003). This approach captures effects of disturbances as well as interannual climate variation on carbon flux. Carbon pools are not explicitly tracked

*Corresponding author.
e-mail: david.turner@oregonstate.edu

in some diagnostic models; thus base rates for key parameters like light use efficiency (LUE), autotrophic respiration (R_a) and R_h must be specified. Because of the relatively low computational costs, diagnostic models are suitable for optimization of multiple parameters using flux tower data (Aalto et al., 2004). A common application for diagnostic NEP models is in generating NEP estimates for comparison (or as 'priors') to top-down flux estimates derived from inversion modelling (e.g. Bousquet et al., 2000).

In this study, we extend the development of an existing diagnostic model for NPP (MOD17; Running et al., 2000) to include R_h, and hence NEP (NPP − R_h). MOD17 employs a LUE approach in its photosynthesis algorithm. LUE approaches trace back to early observations (Montieth, 1972) that NPP is generally related to total absorbed photosynthetically active radiation (APAR). The LUE approach has been widely adopted for scaling GPP and NPP (e.g. Potter et al., 1993; Prince and Goward, 1995) because satellite borne sensors now achieve daily coverage of the Earth's surface at resolutions down to 250 m and reflectance data can be used to derive the fraction of incident PAR that is absorbed by the vegetation canopy. The paper describes new algorithms added to the model, a scheme for parameter optimization, and results of an initial implementation over a heterogeneous region in western Oregon, USA.

2. Methods

2.1. Overview

The carbon flux model, CFLUX, integrates data from multiple sources. Model inputs include daily meteorological data and satellite-derived information on land cover, stand age and FPAR (the fraction of incoming photosynthetically active radiation that is absorbed by the canopy). The processes of gross primary production (GPP), R_a and R_h are treated separately. A simple hydrologic balance is simulated with precipitation, evapotranspiration (ET), and runoff. The time step for the carbon and hydrological cycle processes is daily. Model parameters related to the daily time step responses to weather are optimized against measurements of GPP, NPP, and net ecosystem exchange (NEE) at eddy covariance flux towers, or simulations of these variables with a detailed process-based model. A unique feature for a diagnostic model of this type is that in the case of forest cover types, GPP and R_h are influenced by stand age and stand origin. Thus stand age (a continuous variable) and stand origin (fire or clear-cut) are standard inputs for forested grid cells. Model parameters related to the relatively slow changes associated with stand age are calibrated with the trends in GPP and R_h in a detailed process-based model run over the course of secondary succession. Model parameters are listed in Table 1. For this study, CFLUX was applied at the 1 km spatial resolution over a 10.9 × 10^4 km^2 area in western Oregon, USA (Fig. 1) for the years 2002 and 2003.

2.2. Model Algorithms

The GPP algorithm uses a LUE approach.

$$GPR = eg * \downarrow\text{PAR} * \text{FPAR}, \tag{1}$$

where

GPP = gross primary production (gC m^{-2} d^{-1})
e_g = final LUE (gC MJ^{-1})
↓PAR = incident photosynthetically active radiation (MJ m^{-2} d^{-1})
FPAR = fraction of ↓PAR absorbed by the canopy.

The value e_g is influenced by the degree of cloudiness, the 24 hr minimum temperature (Tmin), the daytime average vapour pressure deficit (VPD), the soil water status (SW) and the stand age (SA).

$$e_g = e_{g\_base} * S_{T\min} * S_{VPD} * S_{SWg} * S_{SAg}, \tag{2}$$

where

e_g = final LUE (gC MJ^{-1}),
e_{g_base} = LUE as influenced by cloudiness (gC MJ^{-1}),
$S_{T\min}$ = minimum temperature scalar (0–1),
S_{VPD} = vapour pressure deficit scalar (0–1),
S_{SWg} = soil water scalar (0–1) and
S_{SAg} = stand age scalar (0–1).

The procedure for determination of e_{g-base} is described in Appendix A. The scalars for minimum temperature and vapour pressure deficit are formulated as in Running et al. (2000) with a linear ramp (1 to 0) between a value when the influence is at a minimum and a value when it is at a maximum (i.e. when LUE is reduced to 0). The scalar for the influence of soil water is based on the ratio of current soil water content to soil water holding capacity (WHC). When the ratio is above a value of 0.5, S_{SWg} is set to 1.0 (no influence) and below a ratio of 0.5 there is a linear ramp from S_{SWg} of one to an S_{SWg} of zero as the ratio hits zero. In the case of forest cover types, a scalar for the effect of stand age on GPP (Appendix B) is implemented to reflect observations of reduced NPP in older stands (Van Tuyl et al., 2005).

The R_a algorithm separates maintenance respiration (R_m) from growth respiration (R_g). The R_m component uses a base rate and a Q_{10} function driven by average daily temperature. The R_m rate is scaled with FPAR because increasing PAR absorbance is associated with increasing live biomass (here following the Beer's Law relationship of FPAR to leaf area index).

$$R_m = R_{m\_base} * Q_{10}^{((T_{air}-20)/10)} * (1/-k)(\log(1-\text{FPAR})) \tag{3}$$

where

R_{m_base} = base rate of maintenance respiration (gC m^{-2} d^{-1}),

Table 1. Summary of CFLUX variables and parameters

Symbol	Description	Units	Source
GPP	Gross primary production	$gC\ m^{-2}\ d^{-1}$	Model output
e_g	Final light use efficiency for GPP	$gC\ MJ^{-1}$	Function (Equation 2)
e_{g_base}	e_g as influenced by cloudiness	$gC\ MJ^{-1}$	Function (Appendix A)
$\downarrow PAR$	Incident photosynthetically active radiation	$MJ\ m^{-2}\ d^{-1}$	Meteorological Input
FPAR	Fraction of $\downarrow PAR$ absorbed by the canopy	0–1	Satellite-borne sensor data
$FPAR_{min}$	Minimum value for FPAR	0–1	Optimized
$FPAR_{df}$	Default FPAR	0–1	Calibrated
S_{Tmin}	Scalar for minimum temperature effect on e_{g-base}	0–1	Function with optimized coefficients
S_{VPD}	Scalar for vapour pressure deficit effect on e_{g-base}	0–1	Function with optimized coefficients
S_{SWg}	Scalar for soil water content effect on e_{g-base}	0–1	Function with calibrated coefficients
S_{SAg}	Scalar for stand age effect on e_{g-base}	0–1	Function with calibrated coefficients
R_a	Autotrophic respiration	$gC\ m^{-2}\ d^{-1}$	Model output
R_m	Maintenance respiration	$gC\ m^{-2}\ d^{-1}$	Function (Equation 3)
R_g	Growth respiration	$gC\ m^{-2}\ d^{-1}$	Function (Equation 4)
R_{m_base}	Base rate of maintenance respiration	$gC\ m^{-2}\ d^{-1}$	Optimized (Equation 3)
Q_{10}	Change in rate for a 10°C increase in temperature	Unitless	Prescribed (here = 2.0)
T_{air}	Daily (24 hr) mean air temperature	°C	Meteorological input
VPD	Vapour pressure deficit	Pa	Meteorological input
Precip	Precipitation	$mm\ d^{-1}$	Meteorological input
k	Radiation extinction coefficient	Unitless	Prescribed (here = 0.5)
R_{g-frac}	Fraction of available C allocated to R_g	0–1	Prescribed (here = 0.33)
NPP	Net primary production	$gC\ m^{-2}\ d^{-1}$	Model output
R_h	Heterotrophic respiration	$gC\ m^{-2}\ d^{-1}$	Model output
R_{h-base}	Base rate of heterotrophic respiration	$gC\ m^{-2}\ d^{-1}$	Optimized (Equation 6)
S_{ST}	Scalar for soil temperature effect on R_{h-base}	0–1	Function with calibrated coefficients (Appendix C)
S_{SWh}	Scalar for soil water content effect on R_{h-base}	0–1	Function with calibrated coefficients (Appendix C)
S_{SAh}	Scalar for stand age effects on R_{h-base}	0–1	Function with calibrated coefficients (Appendix B)
ET	Evapotranspiration	$mm\ d^{-1}$	Model output
WUE	Water use efficiency	$mm\ gC^{-1}$	Prescribed (here = 0.2)
WHC	Soil water holding capacity	mm	Prescribed (here = 200 mm)

Q_{10} = change in rate for a 10°C increase in temperature (here we use 2.0),

T_{air} = daily (24 hr) mean air temperature,

k = radiation extinction coefficient (here we use 0.5) and

FPAR = fraction of $\downarrow PAR$ absorbed by the canopy.

The R_g component of R_a is calculated on a daily basis as:

$$R_g = (GPP - R_m) * R_{g\_frac}, \qquad (4)$$

where

R_{g-frac} is the fraction of carbon available for growth that is used for growth respiration (here we use 0.33, Waring and Running, 1998).

Daily NPP is then:

$$NPP = GPP - R_m - R_g \qquad (5)$$

The R_h algorithm also uses a base rate, and contains functions for sensitivity to temperature, soil moisture, and stand age. As with GPP, a stand age function (Appendix B) is used in the case of forest cover types to reflect the observation of higher R_h

in recently disturbed stands (Campbell et al., 2004). FPAR is included in the R_h algorithm following the logic that annual R_h will track summed FPAR in an equilibrium condition (Reichstein et al., 2003). Including FPAR is also consistent with the observation that a significant proportion of soil respiration is driven by recent photosynthate (Hogberg et al., 2001), which is also driven by FPAR.

$$R_h = R_{h\_base} * S_{ST} * S_{SW} * S_{SA} * FPAR, \qquad (6)$$

where

R_{h_base} = base rate of heterotrophic respiration ($gC\ m^{-2}\ d^{-1}$),

S_{ST} = scalar for soil temperature (Appendix C),

S_{SWh} = scalar for soil water content (Appendix C),

S_{SAh} = stand age factor (Appendix B) and

FPAR = fraction of $\downarrow PAR$ absorbed by the canopy.

A minimum FPAR ($FPAR_{min}$) is specified to permit R_h outside the growing season (e.g. in the cropland/grassland cover type where FPAR may drop to zero). That minimum is determined in
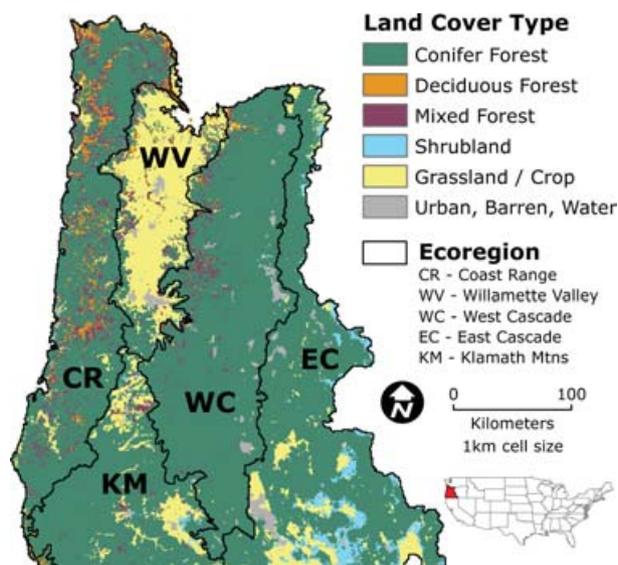
Fig. 1. Map of vegetation cover within Western Oregon, USA study area.

the optimization (see below). In calculating R_h for the conifer cover type, a default FPAR ($FPAR_{df}$) is set below a specified stand age to permit the large R_h fluxes associated with early succession. That default FPAR and the stand age to recovery of full FPAR are specified by forest type within ecoregion, and are derived from the same Biome-BGC simulations as are used for parametrizing the stand age effects on GPP and R_h (Appendix B). For example, minimum FPAR is set to 0.93 and recovery age set to 30 for conifer forests of the West Cascades ecoregion, consistent with local observations (Yang, 2005).

For the simple bucket-type water balance, an estimate of ET is based on GPP and a water use efficiency parameter (mm gC^{-1}). Water use efficiency (WUE) can be determined from observations of GPP and ET at eddy covariance flux towers. Here we used the synthesis studies of (Law et al., 2002) to prescribe WUE by cover type. Soil WHC was assumed to be 200 mm at all locations for this study.

2.3. Parameter optimization

Parameter optimization and calibration was by ecoregion and cover type. The required reference data for the optimization are daily GPP, daily NEE and annual NPP. These data are increasingly reported on a systematic basis at eddy covariance flux towers (Falge et al., 2002; Baldocchi, 2003). However, there was only one active flux tower in the study region, so for this initial application of CFLUX we used outputs from Biome-BGC (Thornton et al., 2002) model runs at representative locations in each ecoregion for all reference data.

The Biome-BGC model runs were based on our previous work with measurements and Biome-BGC simulations in the

region (Law et al., 2001, 2004, 2006; Turner, 2003a; Turner et al., 2004b) In each reference model run, the climate (daily precipitation, Tmin, maximum temperature, VPD and solar radiation) were from a database of DAYMET products for the period 1980–2003 (Law et al., 2004). DAYMET is a scheme for interpolating meteorological station data based on a digital elevation map. (Thornton et al., 1997, 2000; Thornton and Running, 1999). Biome-BGC was spun up using a repeating loop of the 23 yr of daily DAYMET data for a given location and run forward to the year 2003. In the case of forests, there were simulated disturbances in 1650 (fire) and 1950 (fire or clear-cut). For the cropland/grassland cover type, the assumption was made that 50% of the aboveground production was harvested and removed from the site. The year 2002 was used in the optimizations because it was close to the 23 yr mean for annual temperature and precipitation.

Initially, a potential range for each CFLUX parameter to be optimized was determined from the literature (Running et al., 2000; White et al., 2000). The maximum value for LUE (Appendix A) and the parameters controlling LUE sensitivity to Tmin and VPD were then simultaneously optimized using daily GPP in the cost function. All possible combinations of the five parameter values over their potential ranges were tested (31 875 combinations). The MODIS FPAR and DAYMET climate used as inputs to CFLUX were for the same location as the Biome-BGC model run and from the same data as was used in the later spatial mode application of CFLUX (see below). Minimum RMSE with respect to the reference GPPs determined the optimum parameter set. The base rate for R_m was then optimized using the annual NPP as a reference. The minimum bias in the annual NPP determined the optimum R_{m-base}. Lastly, the base rate for R_h and the minimum FPAR were optimized using the daily (24 hr) NEE as the reference values, and the minimum RMSE as the selection criteria. To permit minimum FPAR to track maximum FPAR in the later spatial model application, it is the ratio of minimum to maximum FPAR, which is optimized. The maximum FPAR is determined from the FPAR time-series in a pre-processing step.

2.4. Land Cover and Disturbance History

The ecoregion boundaries were developed from the EPA Level III Ecoregions of the Conterminous United States (http://www.epa.gov/wed/pages/ecoregions.htm). For the purposes of our modelling, an adjustment was made in the boundary separating the EC and WC ecoregions along the crest of the Cascades Mountains to accommodate a different boundary used in our mapping of stand age.

The land cover data layer (Fig. 1) was based on the year 2000 forest cover map in Law et al. (2004) and filling in of non-forest cover types with the 1992 USGS National Land Cover Data (NLCD) layer (http://landcover.usgs.gov/natllandcover.asp). The two data sets were combined and reclassified into six cover

types. The original resolution of the land cover data was 25 m but a majority filter resampling was applied to match the 1 km resolution of the climate and FPAR data (see below).

The stand age and disturbance history surfaces were also from Landsat data and for the 2002 model run were from Law et al. (2004). For the 2003 model run, recent wall-to-wall Landsat Thematic Mapper data for late 2002 was acquired and the change detection approach (Cohen et al., 2002) was used to do an update. The stand age data layer was resampled to 1 km resolution by calculating the mean stand age of 25 m pixels corresponding to the majority land cover type within a 1 km pixel. The disturbance data layer (fire or clear-cut) was resampled to 1 km resolution by determining the dominant 25 m disturbance type corresponding to the majority land cover type within a 1 km pixel.

2.5. Climate Data

The climate inputs to CFLUX are Precip, Tmin, 24 hr average temperature (Tavg), VPD and PAR. These data for 2002 and 2003 were extracted from our DAYMET database (Thornton et al., 1997; Thornton and Running, 1999; Law et al., 2004). The spatial resolution of that database is 1 km. Two additional climate related variables—the soil temperature and the cloudiness index—were prepared in a pre-processing step. Soil temperature was calculated as the mean of Tavg for the previous 25 d. The cloudiness index was calculated as ↓PAR divided by simulated clear sky ↓PAR (See Appendix A).

2.6. FPAR

MODIS FPAR at a 1 km spatial resolution and 8 d temporal resolution for the period 2002–2003 were downloaded from NASA's Earth Observing Data Gateway (http://delenn. gsfc.nasa.gov/~imswww/pub/imswelcome/). The original data were in the Integerized Sinusoidal Projection and were reprojected into the Universal Transverse Mercator Projection (Cohen et al., 2003). Where cloudiness prevented recovery of realistic FPARs, the data were filled in using the approach of Zhao et al. (2005).

3. Results

3.1. Model Inputs

The land cover in the study region (Fig. 1) is predominantly forest with a few large areas that are grassland/cropland, shrubland, urban or barren (high elevations). Most of the forests are coniferous, but in the Coast Range ecozone there are significant areas dominated by red alder (*Alnus rubra*) and big leaf maple (*Acer macrophyllum*). The majority filter to 1 km resolution had the effect of increasing the most frequent class (conifer forest)
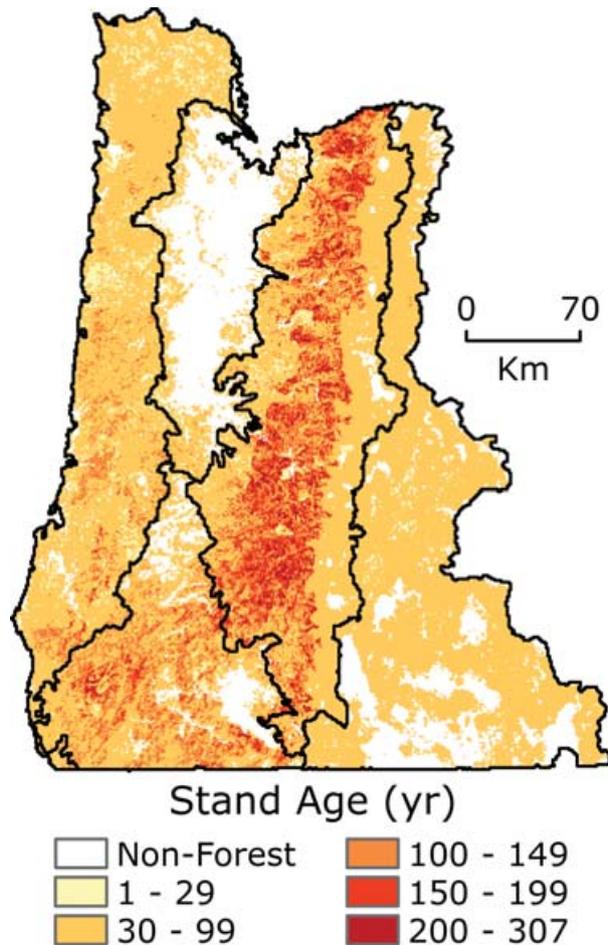
Fig. 2. Map of stand age within study area.

from 62% to 75%. Much of that gain was from the Mixed and deciduous forest classes.

Stand age at the 1 km resolution (Fig. 2) was relatively low in the Coast Range ecozone, where large areas of private land are managed for timber production. It was relatively high in the West Cascades ecoregion that is predominantly public land where significant areas of older forest remain (Van Tuyl et al., 2005). The sharp north–south break in stand age near the crest of the Cascade Mountains is somewhat artificial in that it is the line east of which it was not possible to resolve stand age in conifer stands >30 yr of age with remote sensing. Thus all stands greater than 30 yr of age were mapped as a single age east of that break (Law et al., 2004). The effect of aggregating stand age to the 1 km resolution was to reduce the area of very young forests because most clear-cuts in this region are less that 1 km^2 (Turner et al., 2000). Any single 1 km grid cell might combine very young and older ages. The total area of conifer forest with age less than 30 was 18 percent of forested area at 25 m resolution and 5 percent at 1 km resolution.

Table 2. Ecoregion mean values for annual precipitation and mean annual temperature (MAT)

	Annual Precipitation (mm)		MAT (°C)	
	2002	2003	2002	2003
Ecoregion				
Coast Range (CR)	1986	2168	9.7	10.4
Willamette Valley (WV)	1283	1462	11.2	11.9
West Cascades (WC)	1426	1732	8.2	8.9
East Cascades (EC)	646	847	6.3	7.1
Klamath Mountains (KM)	1154	1241	10.6	11.0

The aggregated climate data shows the west to east gradient of decreasing annual precipitation and mean annual temperature (Table 2). The year 2003 was generally wetter and warmer than 2002, with the biggest differences found in the precipitation increases for the EC and WC ecoregions.

Analysis of the MODIS FPAR data showed a strong season signal in the FPAR for the grassland/cropland areas (Fig. 3a). There was also sensitivity to large fires, such as the one that burned 200 000 ha in southwestern OR in 2002 (Fig. 3b). Plots of FPAR against stand age for conifer grid cells within ecoregions did not reveal a strong relationship (data not shown), suggesting that the 1 km MODIS FPAR is not very sensitive to the relatively small clear-cuts in this region.

3.2. Model Outputs

Results of the Biome-BGC model runs were consistent with the model performance and observations in Law et al. (2004) and Campbell et al. (2004). The optimizations of CFLUX parameters based on these model runs were generally able to reduce bias to nearly zero for annual GPP, NPP and NEP. RMSE values in the daily NEP comparisons (e.g. Fig. 4a) were usually less than 1 gC m^{-2} d^{-1}. Often the disagreements could be related to (1) differences in phenology (in which case the Biome-BGC values could be wrong since model phenology is determined prognostically, (2) problems with the MODIS FPAR, e.g. note the seasonal variation even in dense conifer forests (Fig. 3a) or (3) differences in water balance, which could be related to different rates of ET or assumptions about soil WHC. When calibrated with flux tower data, CFLUX showed quite good agreement with the observations (Fig. 4b).

As expected, the ecoregions differed widely in mean NPP, R_{h}, and NEP (Table 3). The ecoregional patterns in NPP for 2002 showed the effects of the east-west climatic gradient, with the highest NPP in the CR ecoregion (834 gC m^{-2} yr^{-1}) and lowest in the EC ecoregion (350 gC m^{-2} yr^{-1}). Simulated R_{h} was strongly influenced by disturbance history as well as climate and was relatively high in the CR ecoregion because of the young age class distribution and favourable climate.

Mean NEP was similar ($\sim$200 gC m^{-2} yr^{-1}) among the CR, WC and KM ecoregions but lower in the EC ecoregion because
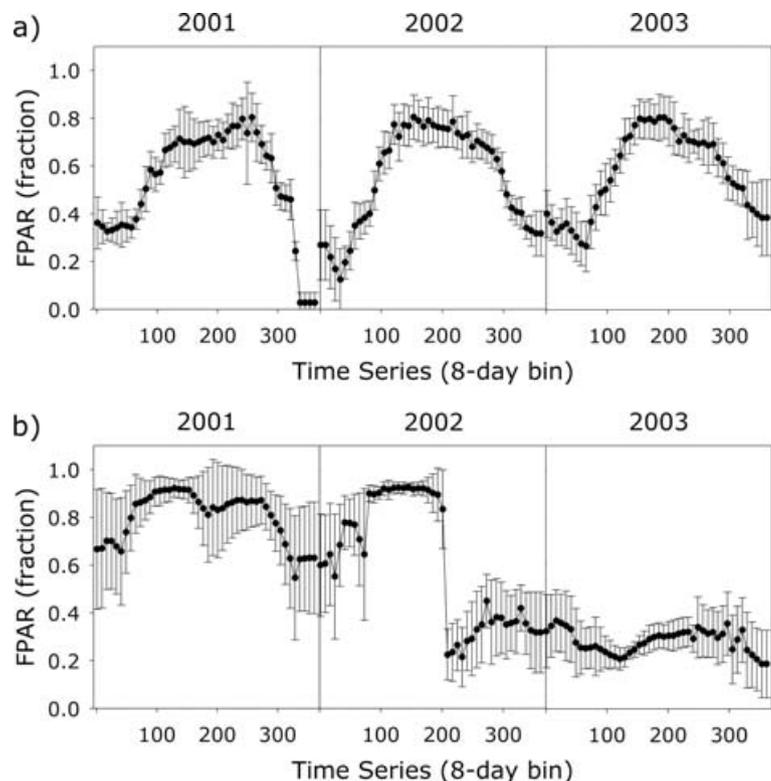
Fig. 3. Three-year trajectory of MODIS FPAR from selected areas within (a) Klamath Basin grassland/cropland and (b) the 2002 Biscuit Fire. The values are means ± the standard deviations of 25 contiguous 1 km² cells.

a) Klamath Mountains 2002

b) East Cascades 2003
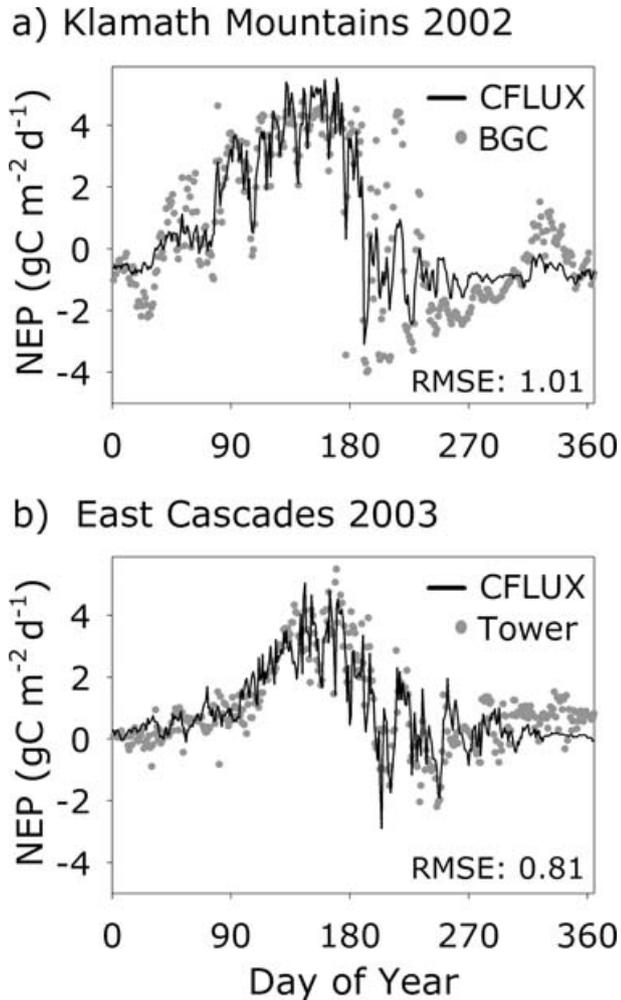
Fig. 4. Daily NEP comparison for the Klamath Mountains (a) and East Cascades (b) conifer forest/clear-cut condition. For the Klamath Mountains case, CFLUX was optimized using Biome-BGC outputs for the site (42°49′N, 123°27′W) as reference data. For the East Cascades case, CFLUX was optimized using observations at the Metolius Mature forest flux tower site (44°27′N, 121°33′W, Irvine et al., 2004).

of climate (Fig. 5). NEP was relatively low in the WV ecoregion, which comprises mostly agricultural crops and grasslands. The carbon sink in agricultural areas traces back to the Biome-BGC simulations used in model parameter optimization (i.e. the assumption made about harvest removals means that input of residues each year is lower than NPP, so R_h tends to be consistently lower than NPP).

The warmer temperatures in 2003 caused NPP to decrease in all ecoregions except the semi-arid EC where a substantial increase in precipitation drove NPP up. NEP likewise decreased everywhere except in the EC ecoregion (Fig. 6), with the biggest drop in the CR ecoregion primarily because of lower NPPs. Over the whole study region, mean NEP decreased from 174 gC m^{-2} yr^{-1} in 2002 to 142 gC m^{-2} yr^{-1} in 2003.

Possibilities for direct validation of large-scale carbon flux estimates are limited. For NPP, estimates have previously been made for 5-yr-average NPP at all plots in the USDA Forest Service Forest Inventory and Analysis (FIA) monitoring network for the study area (Van Tuyl et al., 2005). Specific plot locations are not released for proprietary reasons, so here we compared the ecoregion mean value from the FIA data with the distribution of CFLUX NPPs for all grid cells containing FIA plots within the ecoregion (Fig. 7). The comparisons suggest generally good agreement but a low bias in the CFLUX NPPs for the WC ecoregion. For NEP, we can compare CFLUX estimates with those from Law et al. (2004) based on full implementation of the Biome-BGC model over forested cells in the same study area (Fig. 8). The land cover, stand age and climate data in Law et al. (2004) were from the same sources but the simulation period was the late 1990s and there was no aggregation to 1 km resolution. The comparisons indicate similar sensitivity to differences among the ecoregions and a low bias in the WC ecoregion.

4. Discussion

4.1. Model Algorithms

Relatively simple diagnostic carbon cycle models can take advantage of contemporary data from flux towers and remote sensing. However, a significant challenge is to design algorithms that are responsive to changing conditions but stable over the range of conditions that might be encountered. Simulating the carbon cycle in forests is particularly challenging in this regard because both fast and slow processes must be accommodated and because many forests occur in mountainous terrain with strong environmental gradients.

The fast processes are the day-to-day responses to meteorological conditions. The use of the Tmin scalar and VPD scalars in LUE algorithms such as CFLUX has been shown to be effective over a range of climate regimes (Turner et al., 2005; Turner et al., 2006), especially when calibrated locally and/or supplemented with information on soil water status (Leuning et al., 1995). Previous work with the MOD17 algorithm used in the standard MODIS NPP product (Running et al., 2000) has shown that its lack of responsiveness to overcast conditions frequently caused a low bias in the GPP estimates (Turner et al., 2005). The responsiveness to a cloudiness index in CFLUX addresses this issue, tending to bring LUE up under overcast conditions, which is in line with observations at eddy covariance flux towers (Turner et al., 2003b).

Somewhat slower processes are the regional green-up of non-conifer cover types in the spring, and the soil drought, which typically develops over the course of the summer in the Pacific Northwest. Having FPAR in the CFLUX GPP algorithm helps capture phenology in non-conifer cover types and the inclusion of FPAR in the R_h algorithm is supported by measurements of
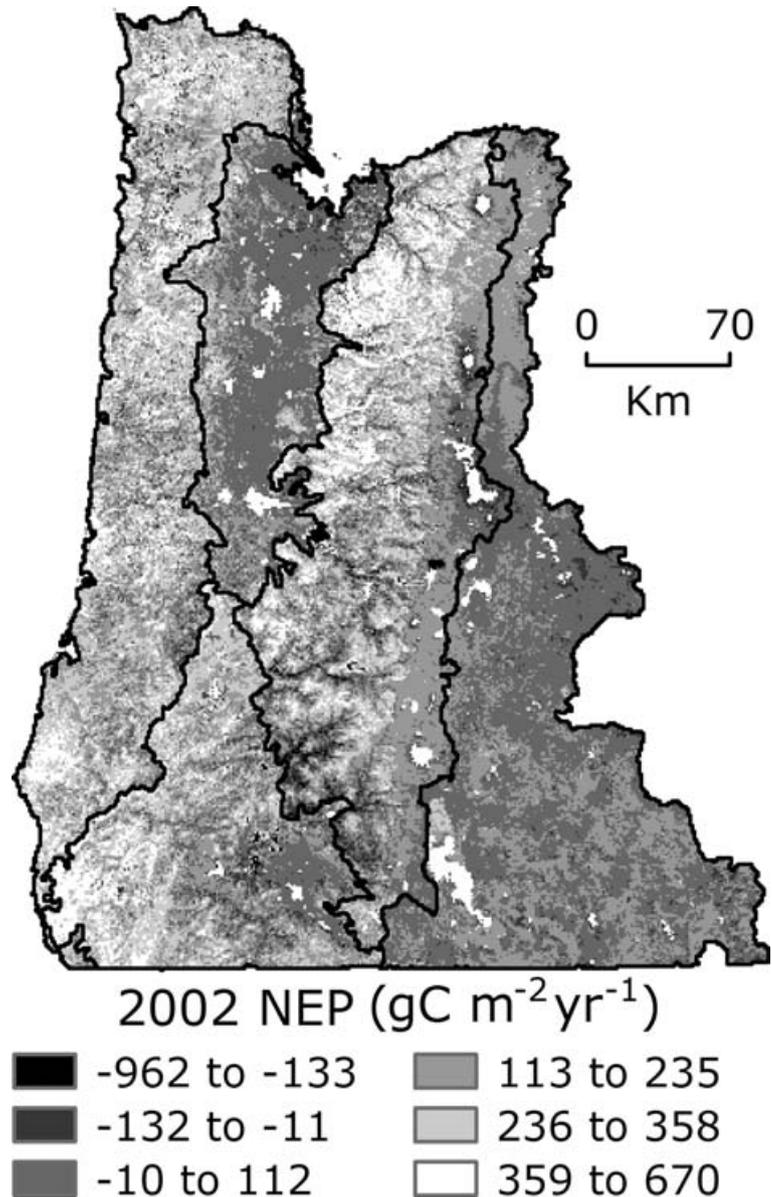
Fig. 5. Net ecosystem production in 2002 for the study area. Positive values are carbon sinks.

soil respiration and FPAR or leaf area index in temperate forests (Reichstein et al., 2003) and in clipped grasslands (Wan and Lou, 2003). Adding a water balance term to both the GPP and R_h algorithms proved to be important in the coniferous forest cover type because soil drought often constrains GPP and R_h in mid to late summer in this region (Runyon et al., 1994; Irvine et al., 2002), without change in FPAR. There is of course additional uncertainty introduced by the requirement of specifying WHC and WUE. These variable were treated in a very simplistic manner for this initial application of CFLUX but in principle could be addressed more rigorously with regional soils databases (Kern et al., 1998) and recourse to local eddy covariance flux data for parametrization of WUE (Irvine et al., 2004; Unsworth et al., 2004).

Interannual variation in climate introduces the next scale of temporal heterogeneity, and in the Pacific Northwest (PNW) is linked in part to the El Niño Southern Oscillation (ENSO) cycle (Greenland, 1994). Studies at eddy covariance flux towers have shown a strong influence of El Niño years on NEP in the PNW. The 2002–2003 period was largely ENSO neutral, but 2003 was generally warmer and wetter over the study area. In Douglas-fir dominated forests, years of high temperature are associated with high ecosystem respiration and decreases in NEP (Morgenstern et al., 2004; Paw U et al., 2004). The results here of decreased NEP in 2003 for the CR, WC and KM ecoregions (predominately Douglas-fir dominated) is consistent with those observations. In Ponderosa pine dominated forests, water balance is probably more important than temperature
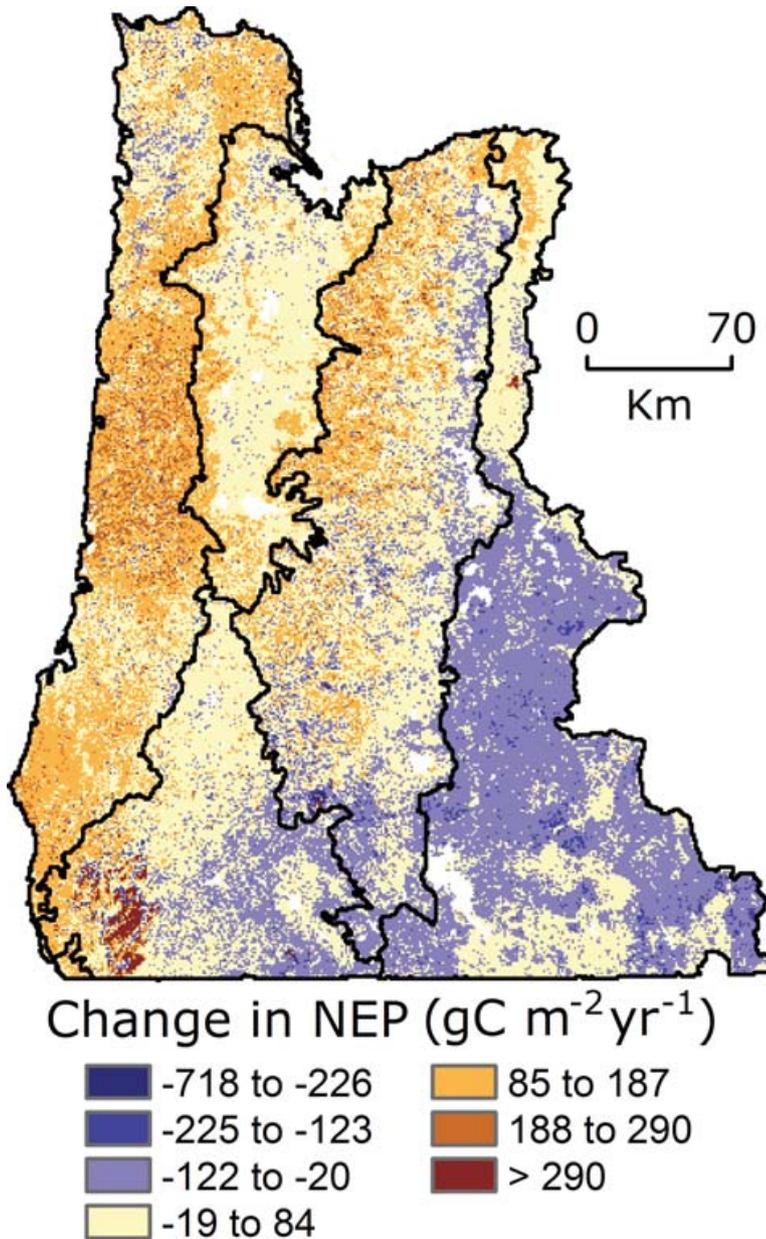
Fig. 6. Map of difference in NEP between 2002 and 2003. NEP for 2003 was subtracted from NEP for 2002. A positive value means 2003 was a larger carbon source or smaller carbon sink than 2002.

(Kusnierczyk and Ettl, 2002) and at flux towers on Ponderosa pine sites relatively dry years are associated with lower NPP and NEP (Law et al., 2000; Mission et al., 2005). That pattern was seen in this study in the higher NPP and NEP is the EC ecoregion in 2003.

The very slow carbon cycle processes that must be treated are the recovery from catastrophic disturbance such as clear-cuts and fire, and the long-term decrease in NPP over the course of succession (independent of FPAR). Chronosequence studies (Acker et al., 2002; Campbell et al., 2004), flux tower studies (Law et al., 2001), and forest inventory studies (Van Tuyl et al., 2005) in the Pacific Northwest have all show strong influences of stand age on NPP and NEP. CFLUX captures the influence of

stand age on NEP by inclusion of scalars derived from outputs of a model that simulates these long-term trends. Key benefits of this meta-modelling approach are in retaining the sensitivity to FPAR, which is lost in prognostic models, and avoiding the computational constraints associated with the Biome-BGC spin-ups (Thornton et al., 2002), which keeps the model nimble enough for optimization of multiple parameters.

4.2. Input Data Layers

The MODIS FPAR product has been checked against ground measurements in only a few cases (Myneni et al., 2002). Over much of Western Oregon the actual value of FPAR is close to 0.9
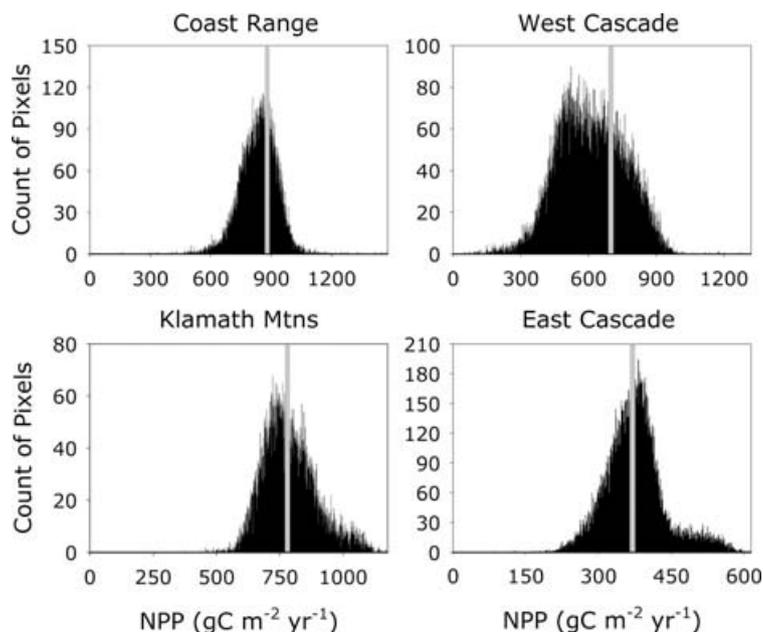
Fig. 7. Histogram of CFLUX 2002 NPP by ecoregion with grey bar representing mean NPP estimates derived from U.S. Forest Service, Forest Inventory Analysis (FIA) plots (Van Tuyl et al., 2005).

because of the dense conifer canopy cover; and inspection of the MODIS FPAR product reveals correspondingly high values. In the drier EC ecoregion, the conifer canopy becomes more open and FPAR should drop. Mean mid-summer FPAR for conifer grid cells in the EC ecoregion was 0.72. However, at the one site in the EC ecoregion where a comparison of ground-based FPAR and MODIS FAR has been made, the ground-based estimate was 0.6 and the MODIS estimate 0.9 (Turner et al., 2005). Possible alternatives to the standard MODIS product include spectral vegetation indices such as the Enhanced Vegetation Index (Xiao et al., 2004), which may have less of a problem with saturation (Huete et al., 2002).

Spatially explicit specification of stand age in regional carbon cycle modelling efforts is challenging but can be done using a variety of approaches (Cohen et al., 1995; Chen et al., 2003). In the PNW, the remote sensing approach reveals the relatively high stand age on public lands (Cohen et al., 2002; Turner et al., 2004b). Since old growth stands (>250 yr of age) tend towards carbon steady state while younger stands (>30) are relatively large carbon sinks (Campbell et al., 2004), this information is essential for monitoring regional NEP. The lower mean NEP in the WC ecoregion compared to the CR ecoregion was driven in part by the larger areas of old-growth forest there (Table 3).

High resolution remote sensing is also capable of distinguishing disturbance type, that is, differentiating fires from clear-cuts (Cohen et al., 2002). There are strong implications for this differentiation when simulating the carbon cycle because of the very different situation with respect to the litter layer and stock of coarse woody debris. Fires generally have the effect of burning off the litter layer, thus setting up the possibility for a small sustained sink as the litter pool is built up in early succession. More important, trees are often killed by forest fire but the biomass is left largely intact, with the net result of sustained carbon source over decades after a disturbance. In contrast, logging typically results in removal of a majority of the biomass, hence the coarse woody debris pool provides a substantially smaller C source as the system recovers (Turner et al., 1995). Several large-scale fires occurred recently in our western Oregon study area—notably the Biscuit Fire that burned nearly 200 000 ha in 2002. The effect is visible in the southwest corner of the state (Fig. 6) because NEP becomes strongly negative in 2003. Because of the sustained carbon source from areas such as this, it will be important to capture the effects of fires in
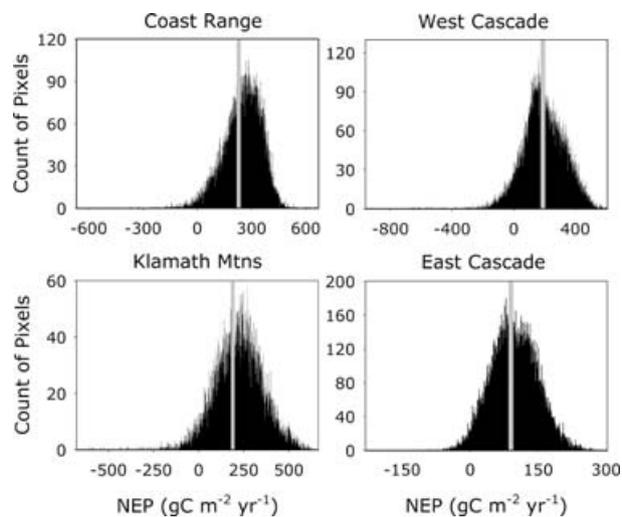
Fig. 8. Histogram of CFLUX 2002 NEP by ecoregion. Grey bars indicate mean NEP for the ecoregion from Law et al. (2004).
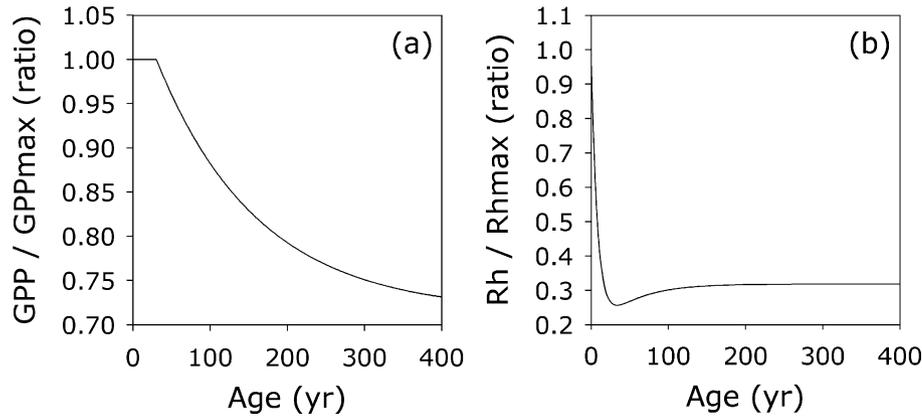
Fig. 9. Stand age effect on (a) gross primary production ($y = a + b*\exp(c * \text{age})$), and (b) heterotrophic respiration ($y = a [0.5 + b*\exp(c * \text{age}) + 0.5 (1 - c^{\text{age}})]$) for the West Cascades-Evergreen Needleleaf-Clear-cut condition.

Table 3. Means values by ecoregion and year for net primary production (NPP), heterotrophic respiration (R_h), and net ecosystem production (NEP). All units are gC m^{-2} y^{-1}

	NPP		R_h		NEP	
	2002	2003	2002	2003	2002	2003
Ecoregion						
Coast Range (CR)	834	732	587	582	246	150
Willamette Valley (WV)	716	688	604	626	113	62
West Cascades (WC)	611	594	419	433	193	166
East Cascades (EC)	350	401	255	270	96	132
Klamath Mountains (KM)	737	723	520	551	210	171
Regional total	625	606	451	405	174	142

biosphere flux models if they are to ultimately be compared with flux estimates based on concentration data.

As noted, the aggregation of stand age to the 1 km resolution had a significant effect on the age distributions, and hence the NEP estimate. Earlier studies in the PNW have suggested that a resolution of ~250 m is needed to resolve the spatial heterogeneity associated with forest management harvesting in this region (Turner et al., 2000). MODIS has channels for the visible and near infrared bands at 250 and 500 m resolutions and that data offers the possibility of more highly resolved FPAR data that would help address the aggregation problem. Schemes for weighting the stand age scalar for a given coarse grain grid cell based on the frequencies of the different ages and their respective scalar values might also be employed.

Examination of the accuracy of the distributed climate data was beyond the scope of this study but previous analyses of diagnostic NPP models have shown significant impacts of uncertainties in distributed climate data on GPP and NPP estimates (Turner et al., 2005; Zhao et al. 2006). Investigation of issues associated with the spatial pattern in soil WHC was also not

possible in this analysis but is warranted especially in relation to simulating R_h.

4.3. Uncertainty in Regional Flux Estimates

Uncertainty in regional flux estimates can be evaluated by comparisons to forest plot data and inventory data (Law et al., 2006), by comparisons to products from other models (e.g. Bachelet et al., 2003), and by checks of observed CO_2 concentration against predicted values when the fluxes are fed into a transport model (Lin et al., 2004).

The grid of field plots supported by the USDA FIA provided an opportunity for comparisons of growth rates and here gave an indication of possible model bias in one of the ecoregions. State-level estimates of net growth (after accounting for mortality) from FIA data (e.g. Table 36 in Smith et al., 2004) suggest live tree carbon is increasing significantly in Oregon in recent years, even after accounting for harvest removals. This accumulation is primarily on public lands where harvesting has been greatly reduced since ~1990. Private lands are approaching an even age class distribution of stands such that NEP is high because of rapid tree growth, even though Net Biome Production (Schulze et al., 2000) is low because much of the stem wood is being removed by harvesting.

The comparisons of CFLUX products to Biome-BGC outputs confirmed that the diagnostic model was largely emulating the results of the prognostic model over forested areas. Flux tower observations would provide more reliable reference data for optimizing the ecophysiological parameters in CFLUX, so it is desirable that systematic collection of tower data be continued.

As yet, there are no regionally resolved inverse modelling flux estimates for our study area. It should ultimately be possible with these analyses to isolate NEP at the regional scale from the other surface fluxes, notably fossil fuel emissions and direct emissions from forest fires. Continental scale inversions report a large but temporally varying carbon sink in temperate North America (Bousquet et al., 2000). The results of this scaling study

in the PNW suggest that the region is contributing significantly to that sink.

5. Conclusions

Spatially and temporally explicit assessments of terrestrial NEP at the regional scale are needed to understand the influence of disturbance and climate on carbon flux and for evaluation of flux estimates based on top down approaches. Because stand age and disturbance history have significant effects on NPP and R_h in forested regions, a bottom-up NEP scaling approach must ideally include such information. Here we developed and tested a diagnostic NEP model (CFLUX) that accounts for spatial and temporal patterns in climate and vegetation FPAR, as well as influences of stand age and disturbance history. With parametrization at the ecoregion scale based on model runs of Biome-BGC over a full successional cycle, this monitoring approach captures the important features of spatial and temporal heterogeneity in regional NEP. Increased attention is needed to issues related to the effects of spatial aggregation of model inputs, uncertainty in model parameters and validation of large-scale flux estimates.

6. Acknowledgments

7. Appendix A. The Influence of Cloudiness

Observations at flux towers representing a variety of biomes have commonly found an increase in LUE under overcast conditions, at both the hourly and daily time steps (Turner et al., 2003b). To account for this pervasive response, an index of cloudiness is calculated and allowed to influence the base rate of LUE in CFLUX.

First an index of cloudiness is created based on observed and potential PAR.

$$CI = 1 - (\downarrow PAR / \downarrow PAR_{po}),$$

where

CI = cloudiness index,
$\downarrow PAR$ = incident PAR (MJ/d) and
$\downarrow PAR_{po}$ = potential incident PAR (MJ/d).

The potential PAR is derived from the algorithm of Fu and Rich (1999) and actual $\downarrow PAR$ is from DAYMET.

A cloudiness index scalar is then created in the form:

$$S_{CI} = (CI_d - CI_{min})/(CI_{max} - CI_{min}),$$

where

S_{CI} = cloudiness index scalar,
CI_d = cloudiness index for the specific day,
CI_{min} = minimum cloudiness index for the year and
CI_{max} = maximum cloudiness index for the year.

The S_{CI} is then used to determine base LUE for a given day.

$$e_{g\_base} = (((e_{g\_max} - e_{g\_cs}) * S_{CI}) + e_{g\_cs}),$$

where

e_{g_base} = base LUE,
e_{g_max} = maximum LUE, an optimized parameter,
e_{g_cs} = clear sky LUE,
S_{CI} = cloudiness index,

e_{g_cs} is calculated as the mean e_g for days with $S_{Tmin} = 1$, $S_{VPD} = 1$ and $S_{SWg} = 1$ and $S_{CI} < 0.2$. This could be from observations at a flux tower or outputs from a physiologically based model.

8. Appendix B. Parametrization of age functions for GPP and R_h

In the case of forested land cover types, the functions specifying age effects on GPP and R_h are calibrated with output from another model—Biome-BGC (Thornton et al. 2002).

The Biome-BGC model was designed to simulate the carbon cycle, nitrogen, and hydrologic cycles over the course of primary and secondary succession and has been extensively tested in the western Oregon study area (Law et al., 2001, 2004, 2006; Thornton et al., 2002; Turner et al., 2003a, 2004b). The model is initially spun-up over an approximately 1000 yr period to bring the C pools into near steady state. A disturbance event, either clear-cut (70% of biomass assumed removed) or fire (all forest floor and 30% of biomass assumed burned off) is then simulated, and the model run forward over the course of secondary succession with annual outputs of GPP and R_h. These data are normalized to a range of zero to one and then used to fit the age effect functions (e.g. Figs. 9a and b). GPP/GPPmax is the scalar for stand age effect on light use efficiency (S_{SAg}). R_h/Rhmax is the scalar for the stand age effect on heterotrophic respiration (S_{SAh}).

9. Appendix C. Effects of soil temperature and moisture on R_h

The general formulation of the R_h algorithm is:

$$R_h = R_{h\_base} * S_{ST} * S_{SW} * S_{SA} * FPAR \quad (eq. 6, \text{ where})$$

$$S_{ST} = e^{(a * Tsoil)}$$

Law, B. E., Turner, D. P., Lefsky, M., Campbell, J., Guzy, M. and co-authors. 2006. Carbon fluxes across regions: observational constraints at multiple scale. In: *Scaling and Uncertainty Analysis in Ecology: Methods and Applications*. (eds. J. Wu, K. B. Jones, H. Li, O. L. Loucks), Columbia University Press, New York.

Leuning, R., Kelliher, F. M., DePury, D. G. G. and Schultze, E.-D. 1995. Leaf nitrogen, photosynthesis, conductance and transpiration: scaling from leaves to canopies. *Plant Cell Environ.* **18**, 1183–1200.

Levy, P. E., Grelle, A., Lindroth, A., Molder, M., Jarvis, P. G. and co-authors. 1999. Regional-scale CO_2 fluxes over central Sweden by a boundary layer budget method. *Agric. Forest Meteorol.* **98-9**, 169–180.

Lin, J. C., Gerbig, C., Wofsy, S. C., Andrews, A. E., Daube, B. C. and co-authors. 2004. Measuring fluxes of trace gases at regional scales by Lagrangian observations: application to the CO2 Budget and Rectification Airborne (COBRA) stud$_8$y. *J. Geophys. Res.-Atmos.* **109** JGR 109 (D15304) doi:10, 10291 2004 JD004754

Mission, L., Tang, J., Xu, M., McKay, M. and Goldstein, A. 2005. Influences of recovery from clear-cut, climate variability, and thinning on the carbon balance of a young ponderosa pine plantation. *Agric. Forest Meteorol.* **130**, 207–222.

Montieth, J. L. 1972. Solar radiation and production in tropical ecosystems. *J. Appl. Ecol.* **9**, 747–766.

Morgenstern, K., Black, T. A., Humphreys, E. R., Griffis, T. J., Drewitt, G. B. and co-authors. 2004. Sensitivity and uncertainty of the carbon balance of a Pacific Northwest Douglas-fir forest during an El-Nino/LaNina cycle. *Agric. Forest Meteorol.* **123**, 201–219.

Myneni, R., Hoffman, R., Knyazikhin, Y., Privette, J., Glassy, J. and co-authors. 2002. Global products of vegetation leaf area and fraction absorbed PAR from one year of MODIS data. *Remote Sens. Environ.* **76**, 139–155.

Paw U, K. T., Falk, M., Suchanek, T. H., Ustin, S. L., Chen, J. and co-authors. 2004. Carbon dioxide exchange between an old-growth forest and the atmosphere. *Ecosystems* **7**, 513–524.

Potter, C., Klooster, S., Steinbach, M., Tan, P., Kumar, V. and co-authors. 2003. Global teleconnections of climate to terrestrial carbon flux. *J. Geophys. Res.* **108**, doi:10.1029/2002JD002979.

Potter, C. S., Randerson, J. T., Field, C. B., Matson, P. A., Vitousek, P. M. and co-authors. 1993. Terrestrial ecosystem production, a process model based on global satellite and surface data. *Global Biogeochem. Cy.* **7**, 811–841.

Prince, S. D. and Goward, S. N. 1995. Global primary production: a remote sensing approach. *J. Biogeogr.* **22**, 815–835.

Raupach, M. R., Rayner, P. J., Barrett, D. J., DefFries, R. S., Heimann, M. and co-authors. 2005. Model-data synthesis in terrestrial carbon observation: methods, data requirements and data uncertainty specifications. *Glob. Change Biol.* **11**, 378–397.

Reichstein, M., Tenhunen, J., Roupsard, O., Ourcival, J.-M., Rambal, S. and co-authors. 2003. Inverse modeling of seasonal drought effects on canopy CO_2/H_2O exchange in three Mediterranean ecosystems. *J. Geophys. Res.* **108**, 1–16.

Running, S. W., Thornton, P. E., Nemani, R. and Glassy, J. M. 2000. Global terrestrial gross and net primary production from the Earth Observing System. In: *Methods in Ecosystem Science* (eds,O. E. Sala, R. B. Jackson, H. A. Mooney and R. W. Howarth) Springer-Verlag, New York, 44–57.

Runyon, J., Waring, R. H., Goward, S. N. and Welles, J. M. 1994. Environmental limits on net primary production and light use efficiency across the Oregon transect. *Ecol. Appl.* **4**, 226–237.

Schimel, D., Melillo, J., Tian, H., McGuire, A. D., Kicklighter, D. and co-authors. 2000. Contribution of increasing CO_2 and climate to carbon storage by ecosystems in the United States. *Science* **287**, 2004–2006.

Schulze, E. D., Wirth, C. and Heimann, M. 2000. Managing forests after Kyoto. *Science* **289**, 2058–2059.

Smith, W. B., Miles, P. D., Vissage, J. S. and Pugh, S. A. 2004. Forest Resources of the United States, 2002. U.S.D.A. Forest Service, North Central Research Station.

Stich, S., Smith, B., Prentice, C. I., Arneth, A., Bondeau, A. and co-authors. 2003. Evaluation of ecosystem dynamics, plant geography, and terrestrial carbon cycling in the LPJ dynamic global vegetation model. *Glob. Change Biol.* **9**, 161–185.

Thornton, P. E., Running, S. W. and White, M. A. 1997. Generating surfaces of daily meteorological variables over large regions of complex terrain. *J. Hydrol.* **190**, 214–251.

Thornton, P. E. and Running, S. W. 1999. An improved algorithm for estimating incident daily solar radiation from measurements of temperature, humidity, and precipitation. *Agric. Forest Meteorol.* **93**, 211–228.

Thornton, P. E., Hasenauer, H. and White, M. A. 2000. Simultaneous estimation of daily solar radiation and humidity from observed temperature and precipitation: an application over complex terrain in Austria. *Agric. Forest Meteorol.*, 255–271.

Thornton, P. E., Law, B. E., Gholz, H. L., Clark, K. L., Falge, E. and co-authors. 2002. Modeling and measuring the effects of disturbance history and climate on carbon and water budgets in evergreen needle-leaf forests. *Agric. Forest Meteorol.* **113**, 185–222.

Turner, D. P., Koerper, G. J., Harmon, M. E. and Lee, J. J. 1995. A carbon budget for forests of the conterminous United States. *Ecol. Appl.* **5**, 421–436.

Turner, D. P., Cohen, W. B. and Kennedy, R. E. 2000. Alternative spatial resolutions and estimation of carbon flux over a managed forest landscape in western Oregon. *Land. Ecol.* **15**, 441–452.

Turner, D. P., Guzy, M., Lefsky, M. A., Van Tuyl, S., Sun, O. and co-authors. 2003a. Effects of land use and fine-scale environmental heterogeneity on net ecosystem production over a temperate coniferous forest landscape. *Tellus* **55B**, 657–668.

Turner, D. P., Urbanski, S., Wofsy, S. C., Bremer, D. J., Gower, S. T. and co-authors. 2003b. A cross-biome comparison of light use efficiency for gross primary production. *Glob. Change Biol.* **9**, 383–395.

Turner, D. P., Ollinger, S. V. and Kimball, J. S. 2004a. Integrating remote sensing and ecosystem process models for landscape to regional scale analysis of the carbon cycle. *BioScience* **54**, 573–584.

Turner, D. P., Guzy, M., Lefsky, M., Ritts, W., VanTuyl, S. and co-authors. 2004b. Monitoring forest carbon sequestration with remote sensing and carbon cycle modeling. *Environmental Manage.* **4**, 457–466.

Turner, D. P., Ritts, W. D., Cohen, W. B., Maeirsperger, T., Gower, S. T. and co-authors. 2005. Site-level evaluation of satellite-based global terrestrial gross primary production and net primary production monitoring. *Glob. Change Biol.* **11**, 666–684.

Turner, D. P., Ritts, W. D., Zhao, M., Kurc, S. A., Dunn, A. L. and co-authors. 44: 1899–1907. Assessing interannual variation in

MODIS-based estimates of gross primary production. *IEEE T Geosci. Remote Sens*.

Unsworth, M. H., Phillips, N., Link, T., Bond, B. J., Falk, M. and co-authors. 2004. Components and controls of water flux in an old-growth Douglas-fir—western hemlock ecosystem. *Ecosystems* **7**, 468–481.

Van Tuyl, S., Law, B. E., Turner, D. P. and Gitelman, A. I. 2005. Variability in net primary production and carbon storage in biomass across forests—an assessment integrating data from forest inventories, intensive sites, and remote sensing. *Forest. Ecol. Manag.* **209**, 273–291.

Wan, S. and Lou, Y. 2003. Substrate regulation of soil respiration in a tallgrass prairie: results of a clipping and shading experiment. *Global Biogeochem. Cy.* **17**, (1054) doi:10.1029/2002 6B00 1971, 2003.

Waring, R. H. and Running, S. W. 1998. Forest Ecosystems. Academic Press, San Diego, CA.

White, M. A., Thornton, P. E., Running, S. W. and Nemani, R. R. 2000.

Parameterization and sensitivity analysis of the BIOME-BGC terrestrial ecosystem model: net primary productin controls. *Earth Interact.* **4**, 1–85.

Xiao, X., Zhang, Q., Braswell, B. H., Urbanski, S., Boles, S. and co-authors. 2004. Modeling gross primary production of temperate deciduous broadleaf forest using satellite images and climate data. *Remote Sens. Environ.* **91**, 256–270.

Yang, Z. 2005. Modeling early forest succession following clear-cutting in western Oregon. *Can. J. For. Res.* **35**, 1889–1900.

Zhao, M. S., Heinsch, F. A., Nemani, R. R. and Running, S. W. 2005. Improvements of the MODIS terrestrial gross and net primary production global data set. *Remote Sens. Environ.* **95**, 164–176.

Zhao, M. S., Running, S. W., Nemani, R. R. 2006. Sensitivity of moderate resolution imaging spectroradiometer (MODIS) terrestrial primary produciton to the accuracy of meteorological reanalysis. *J. Geophys. Res*. **111**(G01002), doi:10:10:1029/2004JGR000004,2006.